THE UNIVERSITY of EDINBURGH

Edinburgh Research Explorer

Micromagnetics of paleomagnetically significant mineral grains with complex morphology

OPEN ACCESS

Click Here for Full Article

Micromagnetics of paleomagnetically significant mineral grains with complex morphology

W. Williams
School of GeoSciences, University of Edinburgh, Edinburgh EH9 3JW, UK

M. E. Evans
School of GeoSciences, University of Edinburgh, Edinburgh EH9 3JW, UK

*Also at Institute for Geophysical Research, University of Alberta, Edmonton, Alberta T6G 2G7, Canada
(evans@phys.ualberta.ca)*

D. Krása
School of GeoSciences, University of Edinburgh, Edinburgh EH9 3JW, UK

Now at European Research Council, COV2 21/062, Rue de la Loi 200, B-1049 Brussels, Belgium

[1] Micromagnetic calculations relevant to paleomagnetism have generally focused on ideal shapes such as spheres and cubes. However, oxide grains that occur naturally in rocks often have irregular morphologies, highly skeletal dendritic forms being particularly common. To investigate the potential effects of complex grain morphology on magnetic stability, we have carried out two parallel sets of calculations. The first is based on randomly distorted 30–120 nm magnetite spheres. We use a three-dimensional finite element/ boundary integral micromagnetic model able to generate suitable morphologies unrestricted by the regular cell structure required by finite difference models. The second model consists of a 300 nm magnetite octahedron from which most of the material has been removed to leave a small octahedral crystallite at each of the six apices connected by an orthogonal framework of thin rods. The results obtained imply that micromagnetic models currently provide no unambiguous evidence that morphological complexities endow magnetite nanoparticles with enhanced coercivity.

1. Introduction

[2] In recent years, numerous micromagnetic calculations have been undertaken to establish the hysteresis properties and domain states of magnetite nanocrystals, which are of great interest to geophysicists. For the most part the geometries investigated have been rather idealized: spheres, cubes, prisms and octahedra [*Fukuma and Dunlop*, 2006; *Williams and Dunlop*, 1989; *Witt et al.*, 2005; *Yu and Tauxe*, 2008]. But it is commonly observed that iron oxide grains possess complex shapes, such as the skeletal crystals (dendrites) found in many rocks of paleomagnetic significance [*Carmichael and Palmer*, 1968; *Larson et al.*, 1969]. Indeed, grains of this type are the dominant remanence carriers in the basalts comprising oceanic layer 2 [*Ade-Hall*, 1964; *Irving et al.*, 1970; *Wayman and Evans*, 1977; *Gee and Kent*, 1995], the source of the magnetic anomalies so important in the initial discovery of plate tectonics. The distinctive morphology of dendrites is due to compositional supercooling arising from rapid quenching, a well-known phenomenon in the consolidation of metals that is also responsible for the delicate beauty of snowflakes and manganese crystals (see also the Space Shuttle's Isothermal Dendritic Growth Experiment, IDGE).

[3] In geophysics, it has long been argued that dendritic grains are likely to be significant because grain surfaces play a crucial role in determining magnetic behavior, particularly in the very small grains that dominate paleomagnetism [*Stacey and Banerjee*, 1974, p. 110]. In fact, it was the consideration of small irregularly shaped grains that originally brought forth the concept of pseudo-single-domain (PSD) behavior [*Stacey*, 1961]. This early paper already appealed to the dipole moments associated with "very small grains" and "small irregular protuberances on larger grains" as the source of magnetically hard remanence in rocks (for a more recent comprehensive discussion, see *Fabian and Hubert* [1999]). Other factors, such as stress and chemical change, are also known to affect magnetic properties of rocks [*Matzka et al.*, 2003]. But these lie beyond the scope of the present investigation, which is restricted to assessing the role of grain morphology. Here, we report the first results from a series of micromagnetic computations aimed at quantifying the effects of complex grain shapes on domain structure and magnetic stability.

2. Methods

[4] We carried out two parallel sets of calculations, one based on randomly distorted spheres, the other involving a prescribed model dendrite. In the former, irregular surfaces were generated by adding bumps and hollows to the surface of an initially spherical grain of given radius. The amplitude of the departures from the initial surface was varied from ±0.1 to ±0.9 of the radius, and their separation was varied from 5° to 90° (in terms of the angle subtended at the grain's center). The height of the surface above or below the surface of the sphere is linearly interpolated between bumps. To span the SD-PSD size range of interest in paleomagnetism, we studied grains with initial radii of 30 nm, 90 nm and 120 nm. Since magnetic properties are primarily grain volume–dependent, the volume of each modeled grain was renormalized to that of the spherical grain from which it had been derived. In the second approach, we investigated the magnetic behavior of a model dendritic grain consisting of six small (100 nm) crystallites arranged at the apices of a 300 nm octahedron.

[5] We used a three-dimensional finite element/boundary integral (3D-FEBI) micromagnetic computer code [*Williams et al.*, 2006] to derive domain structures and their corresponding hysteresis properties, particularly coercivity. The FEBI algorithm [*Fredkin and Koehler*, 1990] has the flexibility to provide the exact geometry required, unrestricted by the regular cell structure required by finite difference models. All the computations consider pure magnetite having cubic magnetocrystalline anisotropy with $\langle 111 \rangle$ easy directions. Material parameters appropriate to magnetite at room temperature were used, namely saturation magnetization ($M_S = 4.8 \times 10^5$ A m^{-1}), exchange constant (A = 1.34×10^{-11} J m^{-1}) and magnetocrystalline anisotropy (K = 1.24×10^4 J m^{-3}) [*Heider and Williams*, 1988; *Pauthenet and Bochirol*, 1951]. Although thermal fluctuations will not change the stable domain state structures we obtain, they will reduce the predicted coercivity values. However, here we concentrate on those changes both in domain structure and coercive force due only to changes in grain surface geometry, and so we do not include thermal fluctuations in this model. Magnetostriction is also neglected since its effects in magnetite are not significant for most PSD-sized magnetite grains [*Fabian and Heider*, 1996].

[6] The computational scheme starts by first establishing the required surface geometry, and meshing the volume ensuring all tetrahedral elements are of a good quality [*Parthasarathy et al.*, 1994; *Knupp*, 2000]. The free magnetic energy of the
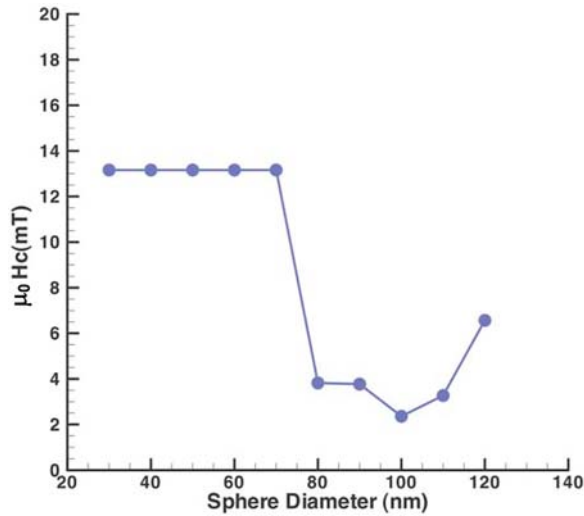
Figure 1. Coercivity as a function of grain diameter for smooth spheres of magnetite. The coercivity data plotted are the averages of the three separate values for fields along the easy, intermediate, and hard axes.

entire grain is the sum of four distinct energy terms:

$$E_{Total} = E_{Exchange} + E_{Crystalline\ Anisotropy} + E_{Demagnetizing} + E_{External\ Field} \qquad (1)$$

A fast initial solution is obtained by minimizing (1), using a conjugate gradient (CG) algorithm [*Williams and Dunlop*, 1989] restarting the CG routine until no further reduction in the energy is achieved. The final equilibrium domain state is then obtained by integrating the Landau-Lifshitz-Gilbert equation of motion for magnetic moments,

$$\frac{d\mathbf{M}}{dt} = -\frac{\gamma}{1+\alpha^2}\mathbf{M} \times \mathbf{H_{eff}} - \frac{\alpha\gamma}{(1+\alpha^2)M_S}\mathbf{M} \times (\mathbf{M} \times \mathbf{H_{eff}}) \qquad (2)$$

where $\mathbf{M}$ is the unit vector along the magnetization direction, γ is the gyromagnetic ratio ($|\gamma| = 2.210175 \times 10^5$ m/As), and α is a damping parameter, which we take as equal to 1.0. $\mathbf{Heff}$ is the effective field acting on the magnetization vector at each node of the finite element mesh, and this is made up from the four constituent fields similar to that for the calculation of the total magnetic energy and is related to the energy by

$$\mathbf{H}_{eff} = -\frac{1}{\mu_0}\frac{dE_{TOTAL}}{d\mathbf{M}} \qquad (3)$$

3. Results

3.1. Choice of Grain Sizes

[7] First, consider the choice of the three grain diameters we investigated. As a benchmark, we derived a preliminary set of micromagnetic models to establish the hysteresis properties of perfect spheres from 30 to 120 nm which covers the single-domain (SD) to pseudo-single-domain (PSD) size range. An instructive pattern emerges (Figure 1). Up to 70 nm, coercivity is constant and corresponds to coherent rotation of uniform magnetization. At 80 nm diameter, the remanence state is still uniform (flower-type), but the magnetization now undergoes incoherent rotation during hysteresis by vortex nucleation and propagation [*Enkin and Williams*, 1994]. A similar switching mechanism exists at 90 nm, except that at this size and above the remanence state is a vortex domain. Beyond 100 nm, coercivity begins to rise again because the majority of the remanence is held within the increasingly dominant vortex core. Here the switching mechanism changes from vortex nucleation and propagation to coherent rotation of the vortex, combined

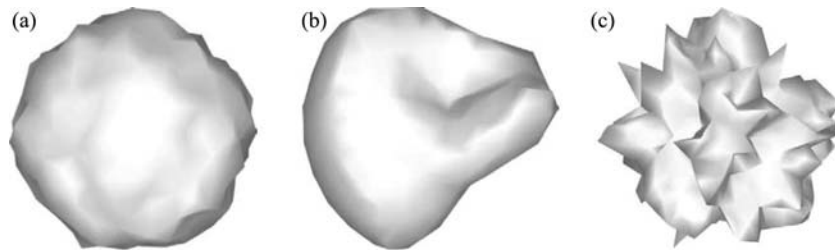**Figure 2.** Some of the grain morphologies examined. These are (a) (0.1,5°), (b) (0.9,90°), and (c) (0.9,5°), where each number pair (A, ϑ) refers to the average bump amplitude (A) above or below the sphere surface, expressed as a fraction of the sphere radius, and the bump wavelength (ϑ) expressed as the average angular separation between bumps subtended at the center of the grain.

with a magnetically softer shell exhibiting incoherent reversal modes.

[8] All these features were confirmed by monitoring the evolution of micromagnetic sequences, but here we restrict attention to the coercivities summarized in Figure 1 because the purpose of these preliminary models was simply to guide the choice of grain sizes to be used in the rest of the investigation. We selected three grain sizes: 30 nm representing an SD grain which undergoes coherent rotation, a 90 nm grain on the PSD boundary, and 120 nm as a stable PSD grain.

3.2. Random Irregularities

[9] Figure 2 shows a representative selection of the grain shapes investigated, arranged in terms of A (the normalized amplitude of the irregularities) and ϑ (their angular spacing). In what follows, it will be convenient to specify a given grain in terms of its (A, ϑ) couplet. Having established the grain morphology, we then derived the micromagnetic domain structures corresponding to fields applied along the $\langle 111 \rangle$ (easy), $\langle 100 \rangle$ (hard), and $\langle 110 \rangle$ (intermediate) axes in a set of simulated hysteresis experiments, with a saturating field of 200 mT. The three hysteresis curves were then averaged, and for each model grain we determined the coercivity (H_C) and the ratio of saturation remanence to saturation magnetization (M_{RS}/M_S). This whole procedure was then repeated for a range of A and ϑ values. In this way, a total of 180 micromagnetic models were analyzed.

[10] The coercivity results are shown in Figures 3a–3c, for the 30 nm, 90 nm, and 120 nm grains, respectively.

3.2.1. The 30 nm Grains

[11] For equidimensional SD grains of this size, we expect the magnetization to be uniform at all values of the applied field, and that the magnetization will switch via coherent rotation. This is, indeed, what
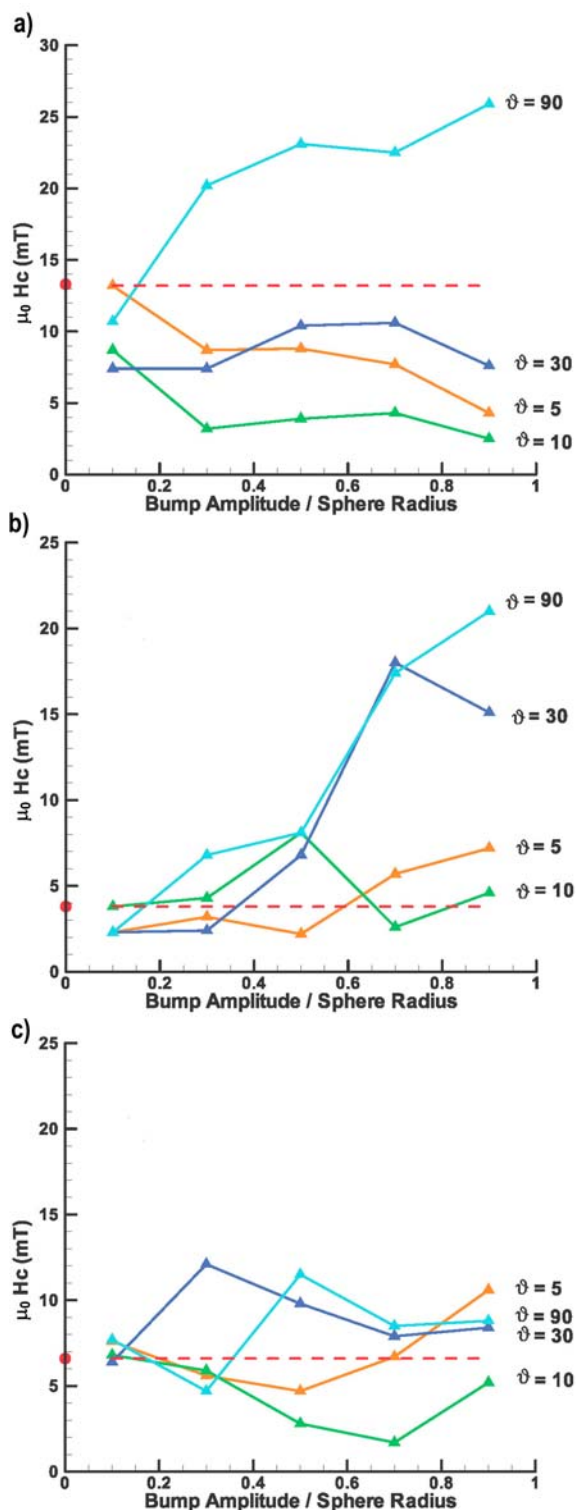

Figure 3. (a) Coercivity (H_C) as a function of average bump amplitude and interbump angular separation for the 30 nm particle. Values of H_C were obtained from the averaged hysteresis curves with field along the [100], [110], and [111] directions. The dashed red line represents the coercivity obtained from a sphere with a smooth surface (as shown in Figure 1). (b) Coercivity (H_C) as a function of average bump amplitude and interbump angular separation for the 90 nm particle. Values of H_C were obtained from the averaged hysteresis curves with field along the [100], [110], and [111] directions. (c) Coercivity (H_C) as a function of average bump amplitude and interbump angular separation for the 120 nm particle. Values of H_C were obtained from the averaged hysteresis curves along the [100], [110], and [111] directions.
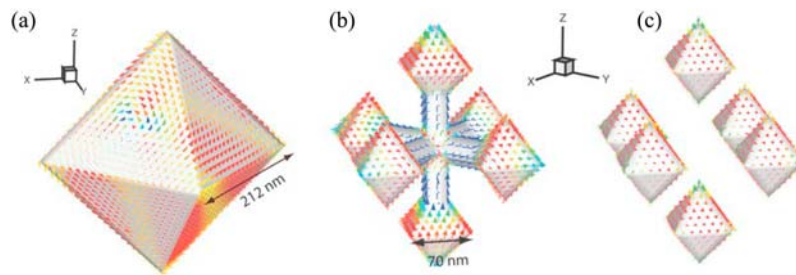
Figure 4. Micromagnetic domain structures for (a) the full octahedron, (b) our model dendrite, and (c) the six independent crystallites.

we observed in the simulation of the smooth 30 nm sphere, for which we obtained H_C = 13.2 mT. This value is lower than analytical value of 20 mT for assemblies of randomly oriented SD magnetite particles [*Dunlop and Özdemir*, 1997, p. 138]. The difference arises because the magnetization within the grain is never perfectly uniform, and even a small degree of flowering will reduce the coercivity.

[12] The effect of adding surface irregularities is generally to reduce coercivity because the bumps act as nucleation points initiating domain reversal. The exception to this is for ϑ = 90°, where the large angular separation, thus small number, of surface bumps means that the grain geometry becomes elongated. This, in turn, gives rise to significant shape anisotropy and increased values of H_C.

3.2.2. The 90 nm Grains

[13] The behavior of the 90 nm grains is dominated by their position just above the SD critical grain size for magnetite. Most grains have H_C values lower than, or similar to, the corresponding SD models. However, as A increases, a tendency for H_C to increase is observed. This can be explained by considering the change in domain state as both the number of surface bumps, and their amplitude, increases. Since the total volume of the grain remains constant, the effect of having a large number of surface bumps is to decrease the effective volume of the grain core. For small values of A, the grain will have a vortex domain state, but as A increases and the bumps account for larger fractions of the grain volume, the core of the grain decreases in size until it can no longer nucleate a vortex domain state and the grains becomes SD Since SD grains have higher coercivities than PSD vortex states, H_C is seen to increase. In addition to this, large values of ϑ introduce significant shape anisotropy, as seen in the 30 nm grain, and this further increases values of H_C.

3.2.3. The 120 nm Grains

[14] The domain state of the 120 nm grains lies firmly in the vortex PSD size range. The effect of surface irregularities on the stability of these larger grains is rather muted. There are occasional quite low values (e.g., 0.7,10°), but the increased stability seen for some of the smaller grains (e.g., ϑ = 90° for 30 nm grains; ϑ = 90° and 30° for 90 nm grains) does not occur.

3.3. Model Dendrite

[15] The modeled morphology is illustrated in Figure 4b, with the corresponding complete 300 nm octahedron and the six separate 100 nm crystallites shown in Figures 4a and 4c, respectively. In Figure 4b the rods connecting the crystallites are aligned along $\langle 100 \rangle$, as dictated by crystal growth kinematics. The whole crystal is very similar to what petrographers call "Maltese cross" grains
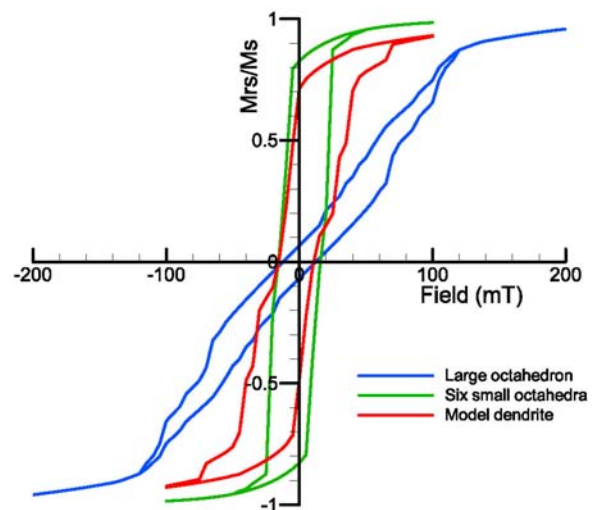

Figure 5. Averaged hysteresis curves formed from fields applied along the [100], [110], and [111] directions for the three octahedral model structures shown in Figure 4.
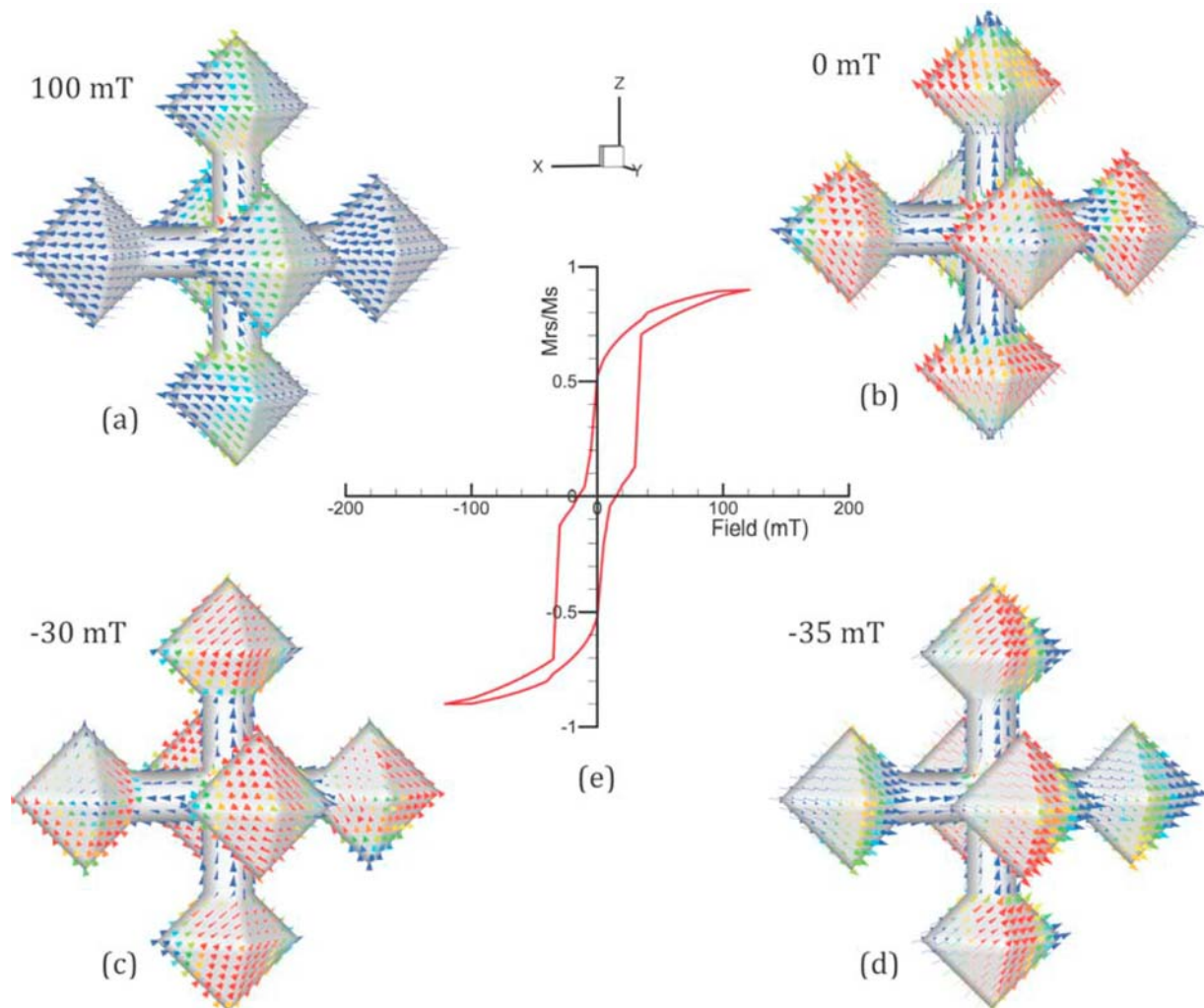
Figure 6. (a–d) Sequence of magnetic structures for the model dendrite during magnetic field cycling shown in the (e) hysteresis loop starting from a field of 100 mT along [100] and progressing to negative field values. At 100 mT (Figure 6a) the magnetization along the [100] field direction is only fully saturated in the crystallites attached to the [100] filament. In the remanence state (Figure 6b), the magnetization of each crystallite relaxes toward its easy direction, but the filaments remain magnetized parallel to their respective axes. Switching of the magnetization occurs at 35 mT (Figure 6d) where the [100] filament and its attached crystallites rotate coherently toward the external field direction.

because of their appearance in two-dimensional polished sections. Looking first at Figure 4a, we find that the zero field magnetization structure after magnetic saturation (SIRM structure) of the full octahedron is characterized by a vortex structure with its core aligned along one of the $\langle 111 \rangle$ directions. Magnetization changes by propagation of the vortex core, and leads to a gradual "ramp-like" hysteresis curve with a low value of 0.07 for M_{RS}/M_S (Figure 5).

[16] It is convenient to consider next the results for the six independent crystallites (Figure 4c). Each crystallite exhibits a weak flower configuration, but they are sufficiently far apart to experience vir-

tually no magnetostatic interaction. Magnetization reverses essentially by coherent rotation, leading to a much "squarer" hysteresis curve (Figure 5) with $M_{RS}/M_S = 0.83$, close to the theoretical value of 0.866 for randomly oriented grains or 0.8 for hysteresis averaged along the three crystalline directions as we have done here.

[17] The behavior of the dendritic grain is more complex (Figure 6). The magnetization of the rods themselves is controlled by their own shape anisotropy and is most easily appreciated by inspecting the sequence of magnetic structures resulting from external field cycling, starting at positive saturating field along [100], stepwise reduction to zero field,
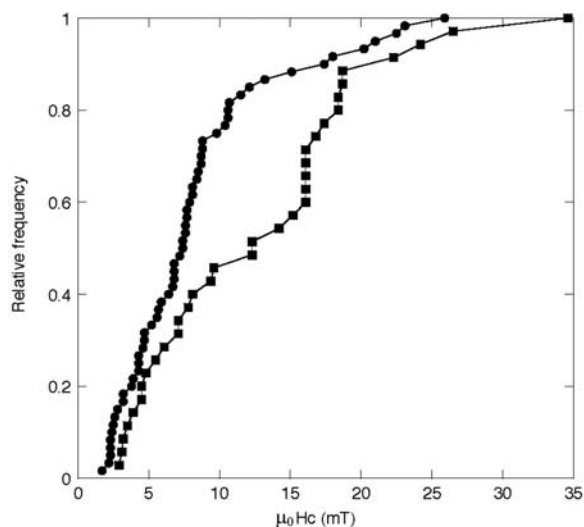
Figure 7. Cumulative distributions of coercivity for our micromagnetic models (circles, N = 60) and for the rock samples studied by *Larson et al.* [1969] (squares, N = 35, compiled from *Larson et al.* [1969, Table 1]).

and subsequent application of an increasing field along [−100]. At an applied field of 100 mT the magnetization of the rods perpendicular to the field remain aligned with their respective rod axes. As the field approaches zero, the magnetization in the crystallites rotates toward the ⟨111⟩ easy axes, but for each crystallite the near perfect ⟨111⟩ magnetocrystalline easy direction alignment observed in Figure 4c is not achieved due to the constraints of the attached rods whose magnetization lies in the hard direction. Furthermore, on applying a reverse field, the magnetization in the rods inhibits complete rotation of the magnetization until a field of −35 mT is applied.

[18] The overall coercivity obtained by averaging the separate values observed for fields along ⟨111⟩, ⟨110⟩ and ⟨100⟩ is roughly the same (∼15 mT) for all three morphologies considered (Figures 5 and 6). However, the M_{RS}/M_S ratio of the dendrite is seven times greater than that of the large octahedron.

4. Discussion and Conclusions

[19] To further assess the micromagnetic results described above, we compare them with published information from real rocks (Figure 7). The data used are taken from what is still one of the most thorough investigations combining relevant rock magnetic measurements with detailed optical microscopy [*Larson et al.*, 1969]. It involves

35 samples (24 basalts, 4 andesites, 3 dolerites, 2 tuffs, 1 diabase, 1 rhyolite) from Japan, California, Oregon and New Mexico. The median value of the cumulative frequency distribution (CFD) of H_C is 12 mT (squares in Figure 7). As is clear from Figure 3, only a handful of the "bumpy grain" models (30 nm, A = 0.3, 0.5, 0.7, 0.9, ϑ = 90°; 90 nm, A = 0.7, 0.9, ϑ = 90° and 30°) yield coercivities significantly greater than the median value obtained from the rock samples.

[20] Closer inspection of Figure 7 suggests that the rock samples actually comprise two separate populations, with H_C above and below ∼15 mT. If the magnetically softer population (N = 19) is analyzed independently, it has a median value of 6 mT, essentially the same as that for the CFD of our micromagnetic results (7 mT, circles in Figure 7). The similarity of the CFD of this softer population and that of the micromagnetic models is striking, and is consistent with the view that irregularities of grain shape control the coercivity spectra of many rocks. We are reluctant to draw such a conclusion, for two reasons. First, our calculations refer to pure magnetite whereas the rock samples are mineralogically more complex (for details, see *Larson et al.* [1969]). Second, we consider nanometric grains well below the optical limit which makes comparison with routine petrographic work hazardous at best. It is possible that the samples studied by Larson and his coauthors contain ultrafine grains like the ones we consider, but we simply do not know. Indeed, there is a pressing need for a new survey using modern electron microscopy to bridge this crucial observational gap.

[21] The magnetically harder population suggested by the rock samples is probably controlled by the occurrence of intergrown crystals in which increased stability arises from physical subdivision of larger grains into magnetite regions separated by ilmenite lamellae. This is borne out by the microscopic work of *Larson et al.* [1969]. It is a well-known phenomenon in rock magnetism (see *Draeger et al.* [2006] for a particularly lucid description of the oxy-exsolution mechanism involved), but is beyond the scope of the present investigation.

[22] In the discussion concerning Figures 3a and 3b, we attributed the cases of higher coercivity to the overall shape anisotropy of grains possessing a relatively small number of large bumps (e.g., 30 nm, ϑ = 90°; 90 nm, ϑ = 90° and 30°). This concept goes back to the analytical work of *Stoner and Wohlfarth* [1948] for grains in the form of ellipsoids of revolution, and has been amply demonstrated micromag-

netically for elongated grains [*Fabian et al.*, 1996; *Tauxe et al.*, 2002; *Yu and Tauxe*, 2008]. It is worthwhile to note that *Tauxe et al.* [2002] consider several other grain morphologies, including one aimed at modeling skeletal grains. This consists of three highly acicular orthogonal "limbs," rather like the inner framework of rods in our dendrite model. They report coercivities on the order of 100 mT, significantly greater than any of the other morphologies they consider. This high coercivity is due entirely to the remanence residing in the highly acicular limbs, which contrasts with our model where the majority of the magnetization lies in the crystallites. The fact that shape anisotropy leads to high coercivity comes as no surprise, but the micromagnetic models we report here indicate that less extreme morphological irregularities do not endow magnetite nanoparticles with enhanced stability.

Acknowledgments

References

Ade-Hall, J. M. (1964), The magnetic properties of some submarine oceanic lavas, *Geophys. J. R. Astron. Soc.*, *9*, 85–92.

Carmichael, C. M., and H. C. Palmer (1968), Paleomagnetism of the Late Triassic, North Mountain Basalt of Nova Scotia, *J. Geophys. Res.*, *73*, 2811–2822, doi:10.1029/JB073i008p02811.

Draeger, U., M. Prévot, T. Poidras, and J. Riisager (2006), Single-domain chemical, thermochemical and thermal remanences in a basaltic rock, *Geophys. J. Int.*, *166*, 12–32, doi:10.1111/j.1365-246X.2006.02862.x.

Dunlop, D. J., and Ö. Özdemir (1997), *Rock Magnetism: Fundamentals and Frontiers*, 573 pp., Cambridge Univ. Press, New York.

Enkin, R. J., and W. Williams (1994), Three-dimensional micromagnetic analysis of stability in fine magnetic grains, *J. Geophys. Res.*, *99*, 611–618, doi:10.1029/93JB02637.

Fabian, K., and F. Heider (1996), How to include magnetostriction in micromagnetic models of titanomagnetite grains, *Geophys. Res. Lett.*, *23*, 2839–2842, doi:10.1029/96GL01429.

Fabian, K., and A. Hubert (1999), Shape-induced pseudo-single-domain remanence, *Geophys. J. Int.*, *138*, 717–726, doi:10.1046/j.1365-246x.1999.00916.x.

Fabian, K., A. Kirchner, W. Williams, F. Heider, T. Leibl, and A. Hubert (1996), Three-dimensional micromagnetic calculations for magnetite using FFT, *Geophys. J. Int.*, *124*, 89–104, doi:10.1111/j.1365-246X.1996.tb06354.x.

Fredkin, D. R., and T. R. Koehler (1990), Hybrid method for computing demagnetizing fields, *IEEE Trans. Magn.*, *26*, 415–417, doi:10.1109/20.106342.

Fukuma, K., and D. J. Dunlop (2006), Three-dimensional micromagnetic modeling of randomly oriented magnetite grains (0.03–03 μm), *J. Geophys. Res.*, *111*, B12S11, doi:10.1029/2006JB004562.

Gee, J., and D. V. Kent (1995), Magnetic hysteresis in young mid-ocean ridge basalts: Dominant cubic anisotropy?, *Geophys. Res. Lett.*, *22*, 551–554, doi:10.1029/95GL00263.

Heider, F., and W. Williams (1988), Note on temperature dependence exchange constant in magnetite, *Geophys. Res. Lett.*, *15*, 184–187, doi:10.1029/GL015i002p00184.

Irving, E., J. K. Park, S. E. Haggerty, F. Aumento, and B. Loncarevic (1970), Magnetism and opaque mineralogy of basalts from the Mid-Atlantic Ridge at 45°N, *Nature*, *228*, 974–976, doi:10.1038/228974a0.

Knupp, P. (2000), Achieving finite element mesh quality via optimization of the Jacobian matrix norm and associated quantities, part I, *Int. J. Numer. Methods Eng.*, *48*, 401–420, doi:10.1002/(SICI)1097-0207(20000530)48:3<401::AID-NME880>3.0.CO;2-D.

Larson, E., M. Ozima, M. Ozima, T. Nagata, and D. Strangway (1969), Stability of remanent magnetization of igneous rocks, *Geophys. J. R. Astron. Soc.*, *17*, 263–292.

Matzka, J., D. Krása, T. Kunzmann, A. Schult, and N. Petersen (2003), Magnetic state of 10–40 Ma old ocean basalt and its implications for natural remanent magnetization, *Earth Planet. Sci. Lett.*, *206*, 541–553, doi:10.1016?S0012-821X(02)01094-4.

Parthasarathy, V. N., C. M. Graichen, and A. F. Hathaway (1994), A comparison of tetrahedron quality measures, *Finite Elem. Anal. Des.*, *15*, 255–261, doi:10.1016/0168-874X(94)90033-7.

Pauthenet, R., and L. Bochirol (1951), Aimantation spontanée des ferrites, *J. Phys. Radium*, *12*, 249–251, doi:10.1051/jphysrad:01951001203024900.

Stacey, F. D. (1961), Theory of the magnetic properties of igneous rocks in alternating fields, *Philos. Mag.*, *6*, 1241–1260, doi:10.1080/14786436108243374.

Stacey, F. D., and S. K. Banerjee (1974), *The Physical Principles of Rock Magnetism*, Elsevier, Amsterdam.

Stoner, E. C., and W. Wohlfarth (1948), A mechanism of magnetic hysteresis in heterogeneous alloys, *Philos. Trans. R. Soc. London, Ser. A*, *240*, 599–642, doi:10.1098/rsta.1948.0007.

Tauxe, L., H. N. Bertram, and C. Seberino (2002), Physical interpretation of hysteresis loops: Micromagnetic modeling of fine particle magnetite, *Geochem. Geophys. Geosyst.*, *3*(10), 1055, doi:10.1029/2001GC000241.

Wayman, M. L., and M. E. Evans (1977), Oxide microstructures and the magnetic properties of Leg 37 basalts, *Can. J. Earth Sci.*, *14*, 656–663.

Williams, W., and D. J. Dunlop (1989), Three-dimensional micromagnetic modelling of ferromagnetic domain structure, *Nature*, *337*, 634–637, doi:10.1038/337634a0.

Williams, W., A. R. Muxworthy, and G. A. Paterson (2006), Configurational anisotropy in single-domain and pseudosingle-domain grains of magnetite, *J. Geophys. Res.*, *111*, B12S13, doi:10.1029/2006JB004556.

Witt, A., K. Fabian, and U. Bleil (2005), Three-dimensional micromagnetic calculations for naturally shaped magnetite: Octahedra and magnetosomes, *Earth Planet. Sci. Lett.*, *233*, 311–324, doi:10.1016/j.epsl.2005.01.043.

Yu, Y., and L. Tauxe (2008), Micromagnetic models of the effect of particle shape on magnetic hysteresis, *Phys. Earth Planet. Inter.*, *169*, 92–99, doi:10.1016/j.pepi.2008.07.006.